

Photometric and Spectral Calibration of the Falcon Telescope Network

C1C Ethan M. Albrecht, C1C Erik G. Jensen,

Kody A. Wilson, Joshua A. Key, Francis K. Chun

USAFA, DFP, 2354 Fairchild Drive, Suite 2A31, USAF Academy, Colorado 80840

Nikola H. Ruby

Imprimis Inc., P O Box 38969, Colorado Springs, Colorado 80937

Murray State University, 102 Curris Center, Murray, KY 42071

David M. Strong

Strong EO Imaging, Inc., 11175 Rocki Ln, Colorado Springs, Colorado 80908

Casey P. Schuetz-Christy

Millennium Engineering & Integration Co., Colorado Springs, Colorado 80919

ABSTRACT

The Falcon Telescope Network (FTN) consists of 0.5-meter, f/8 Officina Stellare ProRC-500 telescopes, six in Colorado, one in Pennsylvania, one in Chile, one in Germany, and two in Australia. These telescope systems have identical hardware components such as the Software Bisque Paramount ME2, an Andor Alta F47 camera, and an Apogee AFW50-9R filter wheel. The filter wheel contains Johnson-Cousin photometric filters (B, V, R) and a 100-lines-per-millimeter Richardson diffraction grating for low-resolution slitless spectroscopy. This paper describes the process and approach we used to photometrically and spectrally calibrate the U.S.-based telescopes in the FTN using standard astronomical techniques and accepted calibration stars, such as Landolt and Oja for photometric calibration and stars with well-known absorption and emission lines for spectral calibration. For the photometric calibration project, we report on the extinction coefficient and zero point for each filter, and for the spectral calibration, we report on the pixel-to-wavelength conversion equation for the diffraction grating.

1. INTRODUCTION

Ground-based, optical observations of satellites are a key component of Space Domain Awareness and support the mission of the United States Space Force [1]. Simultaneous satellite observations from geographically diverse telescope sites can potentially be more effective in characterizing elements of the satellite's orbit and optical properties. However, satellite observations, especially optical signatures, cannot be quantitatively compared without a common basis for comparison. The Falcon Telescope Network (FTN) consists of eleven 0.5-meter, f/8 Officina Stellare ProRC-500 telescopes; six in Colorado, one in Pennsylvania, one in Chile, one in Germany, and two in Australia [2]. These telescope systems have identical hardware components such as the Software Bisque Paramount ME2, an Andor Alta F47 camera, and an Apogee AFW50-9R filter wheel. The filter wheel contains Johnson-Cousin photometric filters (B, V, R) and a 100-lines-per-millimeter Richardson diffraction grating for low-resolution slitless spectroscopy. In this study, we report on the effort to calibrate the photometric and spectral response of several of the U.S.-based FTN telescopes.

The photometric calibration stars were selected from the Landolt and Oja star catalogs and were observed throughout the year. From these calibration stars, the extinction coefficients and zero points of each filter were determined for individual FTN telescopes. Of the seven U.S. FTN telescopes, we were successfully able to observe calibration stars with 6 of the telescopes across 63 nights, resulting in over 10,000 raw images. Those telescopes were located at Otero Junior College (OJC-Falcon), Grand Mesa Observatory associated with Colorado Mesa University (CMU-Falcon),

DISTRIBUTION STATEMENT A: Approved for public release: distribution unlimited. PA#: USAFA-DF-2021-237

Fort Lewis College (FLC-Falcon), Northeastern Junior College (NJC-Falcon), and the Applied Research Lab at Pennsylvania State University (PSU-Falcon). Additionally, we calibrated the 16-inch telescope on the campus of the Air Force Academy (USAFA-16). The spectral calibration of the diffraction grating in an FTN telescope used several stars with well-known absorption lines or in the case of Wolf-Rayet stars, well-known emission lines, which allowed us to determine the pixel-to-wavelength conversion for a telescope. Of the five Falcon telescopes that were photometrically calibrated, we were only able to spectrally calibrate two telescopes, CMU-Falcon and NJC-Falcon for this study.

2. PHOTOMETRIC CALIBRATION METHODS

Photometric calibration was achieved by observing calibration stars (CalStars) of well-known magnitudes. These CalStars were chosen from a catalog of Landolt and Oja CalStars with varying magnitudes and evenly spaced through the sky usually beginning in the West and ending in the East. Fig. 1 illustrates the process used for data collection, processing, and development of calibration parameters. The FTN telescopes are capable of automated collecting when tasked through the Cadet Space Operations Center (CSOC) website. The majority of the collections were made through this process without an operator present. Occasionally however, we did manually operate a telescope. After the collections were made, we would download the data from the CSOC for processing.

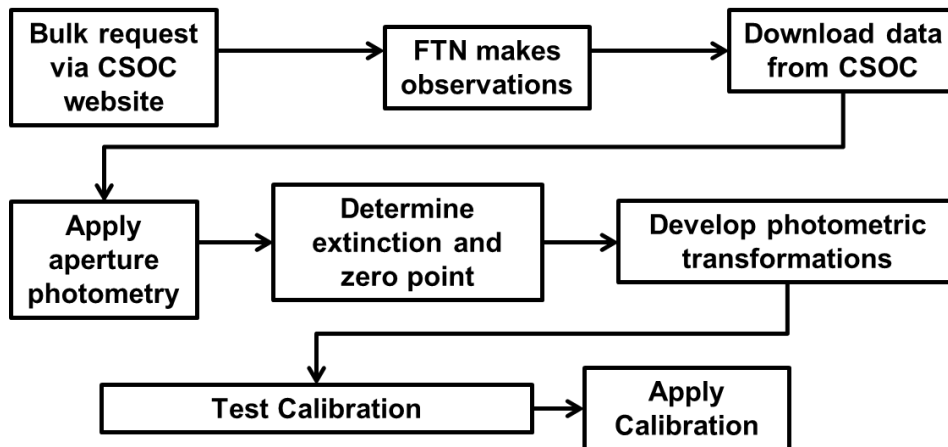


Fig. 1. Processing method for FTN Calibration. Top row shows how a FTN user would collect automated data with the FTN. Middle row shows how the FTN images were processed. Bottom row shows what was done once a calibration curve was made and applied to the data.

The FTN images were processed by Air Force Academy students and researchers using in-house developed software. A curved atmospheric model was used when calculating airmass $M(z_r)$ [3]. The instrument magnitude of each CalStar was determined using standard aperture photometry techniques which uses a signal aperture and a background annulus for each image. The size of the signal aperture for a given CalStar is determined by associating flux measurements more than one standard deviation above the background noise present in the image as part of the star. The inner ring of the background annulus is chosen as 1.5 times the radius of the signal aperture and the outer ring of the background annulus is determined to ensure the signal aperture and background annulus have equal areas. The flux of the CalStar (F_{CalStar}) is calculated by subtracting the counts in the signal aperture by the counts in the background annulus and dividing the net count by exposure time. The instrument magnitude is then calculated via Eq. 1.

$$m_{\text{inst}} = -2.5 \log(F_{\text{CalStar}}) \quad (1)$$

Once a minimum of three or more CalStars are observed by a site for a given filter, the relationship between the instrument magnitude, catalog magnitude, and airmass is determined which is known as the extinction curve. An example extinction curve is shown in Fig. 2 for 07 Jan 2021 for the visible V filter. The slope or extinction coefficient

represents how the instrument and catalog magnitude difference varies as a function of airmass, and the y-intercept or zero point is the predicted smallest magnitude the telescope could detect if no atmosphere was present.

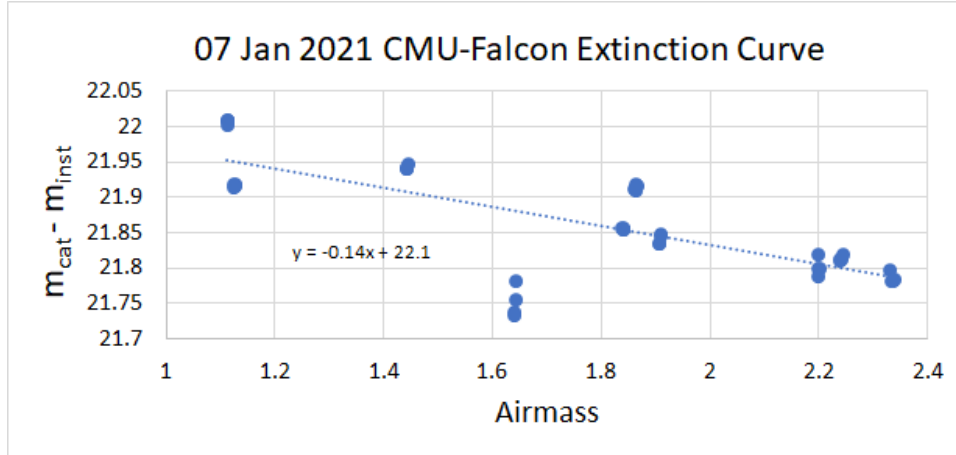


Fig. 2. Extinction curve for CMU-Falcon, V filter. The calculated airmass is on the horizontal axis, and the catalog magnitude minus the instrument magnitude is on the vertical axis for the 10 stars observed on 07 Jan 2021. For this set of data, the extinction coefficient and zero point are -0.14 and 22.1, respectively.

3. SPECTRAL CALIBRATION METHODS

An overview of the spectral calibration process can be seen below in Fig. 3. Images of CalStars are collected using a diffraction grating to create an interference pattern in the image. This interference pattern contains spectral features from the individual CalStars that can be identified and matched to the known wavelengths of these features. Before this can be done, the image must be rotated and clipped to minimize the amount of spectral information that is mixed in the averaging process.

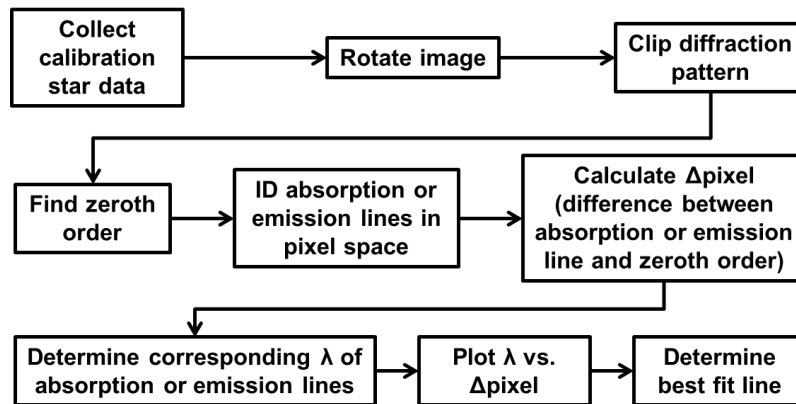


Fig. 3. Overview of spectral calibration process detailing the steps taken to determine the pixel-wavelength relationship for the FTN.

The spectral information from multiple objects in the unresolved imagery was extracted using slitless spectroscopy techniques where a diffraction grating separates incident light into different wavelengths. This occurs because different wavelengths have different angles for constructive interference as described by Eq. 2.

$$D\sin(\theta) = n\lambda \quad (2)$$

where D is the spacing between lines in the slit, θ is the angle along the measurement plane relative to the zeroth-order, n is the order number of the diffraction pattern, and λ is the wavelength. Fig. 4 shows an example of this technique where the diffraction pattern of multiple objects in the field of view are visible. This image was taken using the 100-lines-per-millimeter diffraction grating on the CMU-Falcon telescope which was tracking the Wolf-Rayet star HD 4004. From Fig. 4, one can see that the diffraction pattern is not in perfect alignment with the CCD array, so we need to rotate the raw image to be horizontal (2nd step in Fig. 3) to ensure that spectral information from different wavelengths do not overlap one another when the columns are averaged to obtain a spectra.

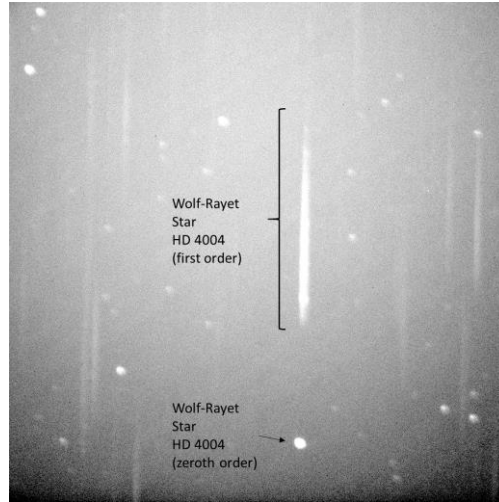


Fig. 4. Image of HD 4004's spectra taken with a 100-line-per-millimeter diffraction grating on the CMU-Falcon telescope.

To correct the alignment we applied a method outlined by Tippets et al [4]. The images for the CMU-Falcon and NJC-Falcon telescopes were rotated, so the the diffraction pattern was approximately horizontal with respect to the rows of the image. This ensured that the spectral information for a particular wavelength was contained within the column of the image, and not spread across multiple columns. Once the image was rotated, it was clipped for averaging the spectra. In this characterization, the clipped images were clipped from 1024x1024 down to 60x1024. With this clipped image, an average diffraction pattern for the calibration stars was produced.

After we clip the image, we identify the location in pixel space of the zero order and any absorption or emission lines in the calibration star's spectra. Before spectral information can be extracted from unknown targets, the system has to be characterized using the spectral features of known sources.

By using these known spectral features, a transformation between pixel space and wavelength space can be obtained as described by Eq 3.

$$\lambda = m * \Delta Pixels + b \quad (3)$$

Where λ is the wavelength, $\Delta Pixels$ is the number of pixels from the zeroth order, m is the slope, and b is an offset to ensure that the wavelength range is from 400-1000 nm. Eq. 3. can be used to map the transform from pixel space to wavelength space, because $\sin(\theta)$ in Eq. 2. is simply the ratio between the $\Delta Pixels$ and the distance from the diffraction grating to the interference feature on the CCD. Given these factors, the conversion only needs to be characterized once for a given telescope as long as the diffraction grating does not change. Additionally, it would be expected the conversions would be the same across identical telescope setups. This can be visually seen in Fig. 5, which displays the virtually identical diffraction patterns created by the gratings in the CMU and NJC telescopes.

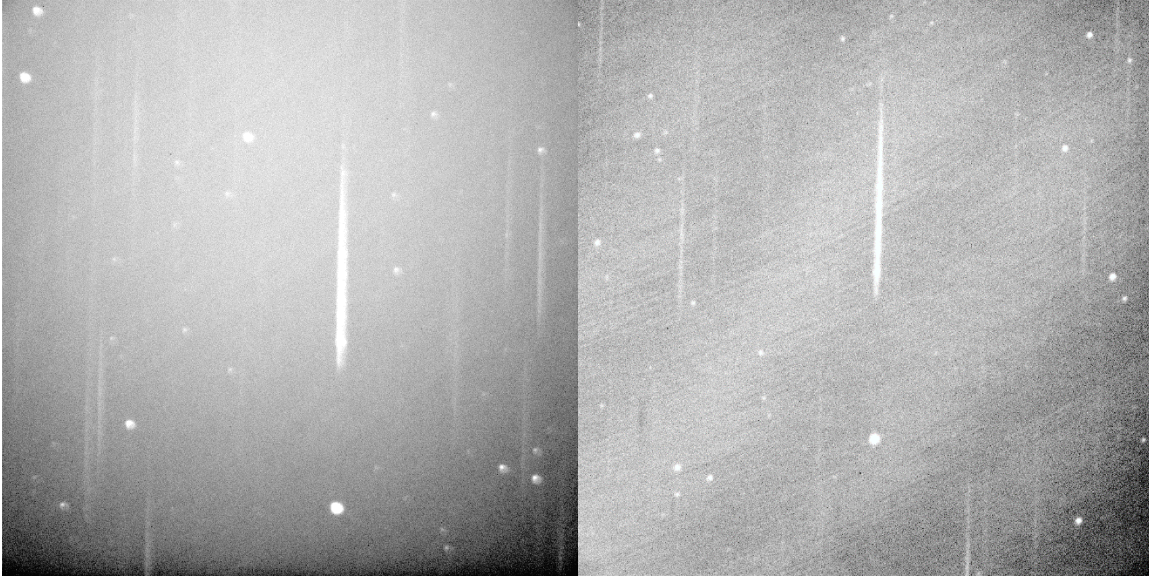


Fig. 5. Diffraction patterns created by HD 4004's spectra taken on Jan 27th 2021 on the CMU-Falcon (left) and NJC-Falcon (right) telescope taken on March 3rd 2021.

4. PHOTOMETRIC RESULTS

The photometric extinction curve parameters are shown in Table 1 for the 20 nights of data collected in 2020-2021 across 6 FTN sites. Blank cells represent data not processed due to having less than three CalStars and the columns on the right-hand side show how many CalStars were collected that night for that filter if processed. Some of the cells in the B-filter column are also blank because we did not start collecting CalStars using the B filter until November 2020. The mean slope and intercept plus/minus the standard deviation of the data for each site across all time is included for each site if multiple nights of data were collected for that site. In the observations, the extinction coefficient (slope) is steeper for the B filter compared to the V and R filters. This is expected as shorter wavelength light is both absorbed and scattered by the atmosphere to a greater extent than longer wavelengths. In this data there is a correlation between an increase in the number of stars and a decrease in slope, as can be seen in Table 1. CMU-Falcon and FLC-Falcon both have similar slopes with a different number of stars. This is believed to be caused by a change in data collection method when collections were made the entire night instead of the first few hours of the night or a property of those unique nights such as season, temperature, humidity, etc. Investigation into this correlation is ongoing.

TABLE 1. 2020-2021 EXTINCTION PARAMETERS

YYYY/MM/DD – Site	B Filter		V Filter		R Filter		# B Stars	# V Stars	# R Stars
	Slope	Intercept	Slope	Intercept	Slope	Intercept			
2020/04/10 – CMU			-0.22	22.17	-0.12	22.27		3	3
2020/04/28 – CMU					-0.19	22.29			3
2020/05/08 – CMU			-0.15	22.05	-0.12	22.16		6	6
2020/12/05 – CMU			-0.05	22.10				14	
2021/01/07 – CMU			-0.14	22.10				10	
CMU Mean±Std			-0.14±0.06	22.11±0.04	-0.14±0.03	22.24±0.06			
2020/02/05 – FLC			-0.18	21.89	-0.12	21.91		3	3
2020/04/10 – FLC			-0.19	21.85	-0.16	21.92		8	7
2020/05/08 – FLC			-0.15	21.77	-0.13	21.85		6	6
2020/11/10 – FLC	-0.42	22.14	-0.23	21.98	-0.21	22.05	5	5	5
2020/11/24 – FLC	-0.38	22.03	-0.17	21.91	-0.19	22.06	4	5	5
2020/11/25 – FLC	-0.42	22.07	-0.16	21.91	-0.14	22.00	4	6	4
2020/12/05 – FLC			-0.05	21.67				29	
2020/12/16 – FLC			-0.11	21.78				15	
FLC Mean±Std	-0.41±0.02	22.08±0.04	-0.16±0.05	21.85±0.09	-0.16±0.03	21.96±0.08			
2020/11/24 – NJC	-0.64	22.10	-0.27	21.68	-0.27	21.79	4	5	5
2020/11/25 – NJC	-0.66	22.09	-0.18	21.56	-0.22	21.78	3	3	3
NJC Mean±Std	-0.65±0.01	22.10±0.01	-0.22±0.05	21.62±0.06	-0.24±0.03	21.79±0.01			
2020/09/04 – PSU			-0.17	21.05	-0.14	21.25		12	12
2020/09/05 – PSU			-0.18	19.60	-0.17	21.18		9	9
2020/09/25 – PSU			-0.19	20.83	-0.16	21.00		13	13
PSU Mean±Std			-0.18±0.01	20.49±0.64	-0.16±0.01	21.14±0.11			
2021/03/19 – OJC			-0.15	21.66				9	
2020/01/23 – USAFA			-0.22	21.58	-0.14	21.58		5	5

For each night, the extinction curves were used to create a calibration function for each filter, and then used to convert instrument magnitudes into calibrated magnitudes using Eq. 4.

$$m_{cal} = kX + m_{zp} + m_{inst} \tag{4}$$

where k is the extinction coefficient for a given photometric filter on a given night, X is the airmass of the object in question, and m_{zp} is the zero point for the filter for that same night. These calibrated magnitudes were then compared to the catalog magnitudes for the 10 observed CalStars as shown in Table 2. for collections made with the CMU-Falcon V filter on 07 Jan 2021. The standard deviation for the 4 images for each CalStar is shown in the 4th row. The average uncertainty in the calibrated magnitude measurements was 0.018 magnitudes. The last row represents the error or the absolute value of the difference between the catalog magnitude and the average calibrated magnitude. The average error across this night for the CMU-Falcon V filter was 0.043 magnitudes.

TABLE 2. CALIBRATION ACCURACY V FILTER CMU-FALCON (07 JAN 2021)

Star Name(HD)	209796	215044	222732	001213	000315	005319	011983	285691	021197	268518
Catalog	8.933	8.503	8.857	8.322	6.440	8.046	8.192	9.454	7.866	7.580
m_{cal}	9.013	8.489	8.793	8.287	6.444	8.044	8.196	9.399	7.994	7.613
Std	0.130	0.003	0.004	0.003	0.011	0.001	0.006	0.003	0.019	0.002
Error	0.079	0.014	0.064	0.035	0.010	0.002	0.006	0.055	0.128	0.033

Achieving the accuracy above requires calibration collections throughout the entire night. This reduces the amount of time spent collecting data on the target of interest. Therefore, we investigated the relationship between the number of CalStars and the average error to determine at what point adding more CalStars doesn't significantly improve our average error. Fig. 6(a) shows that as more CalStars are used to calibrate the night of 07 Jan 2021 a decrease in average error is observed. The night of 07 Jan 2021 is a characteristic curve and shows that after calibrating with the first 4-6 CalStars very little increased accuracy would be gained from adding additional CalStars. This is a feature of the nights examined and the point of diminishing returns was not seen to be more than 6 CalStars on any other night. In Fig. 6(b) the calibration curve was generated using CalStars observed at the end of the night. It can be seen as well that after using the last 4-6 CalStars very little accuracy is gained by increasing the amount of CalStars used. It should be noted that using the stars collected at the end of the night resulted in lower overall accuracy. This is largely due to CalStar #9 being a significant outlier as seen in Fig. 1 just over 1.6 airmass far below the extinction curve. The effect

of this outlier is reduced as more calibration data is used until similar accuracy is seen for calibrating using data at the start of the night as is seen for the end of the night.

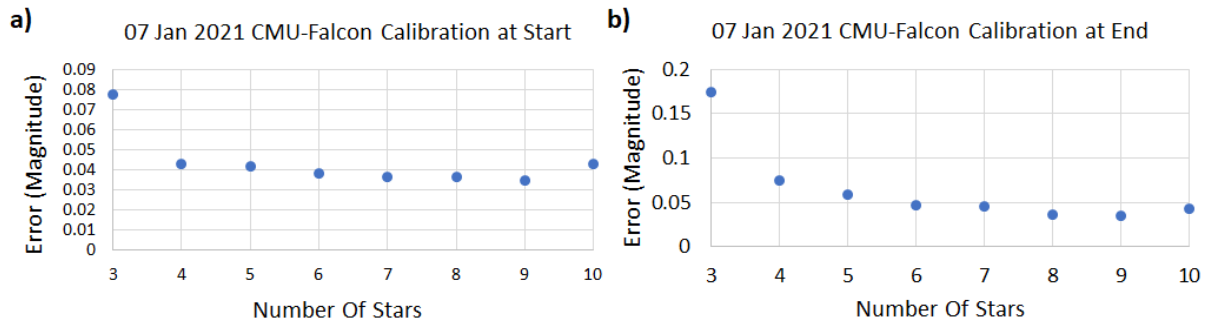


Fig 6. Average error for all stars observed on a night 07 Jan 2021. (a) Shows the average error when the calibration is done using CalStars images from the beginning of the night. (b) Shows the average error when the calibration is done using CalStars images from the end of the night.

In Fig. 7 individual image error is shown for the individual observations in the order of collection on night 07 Jan 2021 across a time span of 3.5 hours. The individual image error is the absolute value of the difference between the catalog magnitude and the calibrated magnitude. Each of the 10 stars shown had 4 images taken consecutively with B, V, and R filters. The first 4 stars or 16 images were used to determine the extinction curve. The error for each image collected that night was then calculated. The error is shown for the V filter in Fig. 7 and a correlation between increased error and increased time since calibration can be seen. The exact nature and root cause of this correlation is still being investigated, however we surmise that it was probably due to a changing night sky resulting in less than ideal photometric sky conditions towards the end of the 3.5 hours.

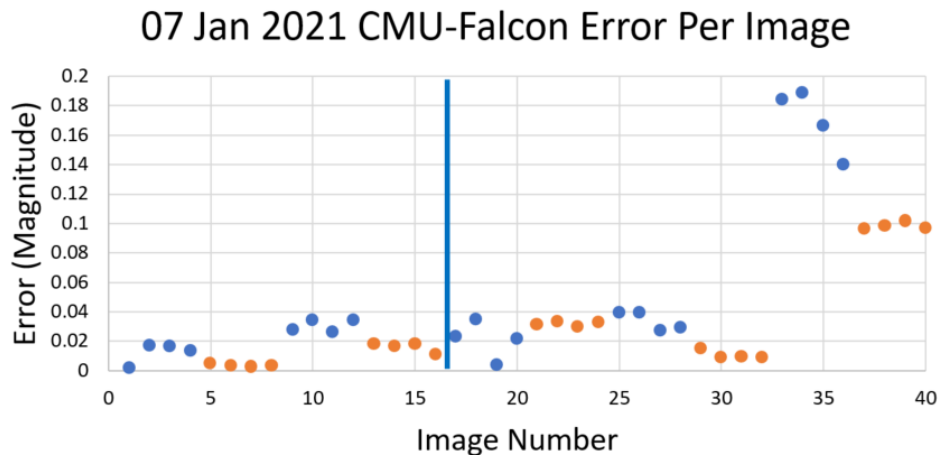


Fig. 7. Error for the individual star observations made on night 07 Jan 2021. The images to the left of the vertical line represent the 4 stars and 16 images that were used to generate the extinction and calibration curves for the night. Each alternating-colored set of 4 data points represents the error from 4 images from a single CalStar.

5. SPECTRAL RESULTS

In this work, 4 stars were used for CMU-Falcon and NJC-Falcon telescopes with a total 17 and 16 spectral features respectively. The stars were Alhena, Sirius, SAO 59570, and HD 4004. HD 4004 is a Wolf Rayet star whose diffraction pattern in pixel space and the wavelengths of prominent emission features can be seen below in Fig. 8.

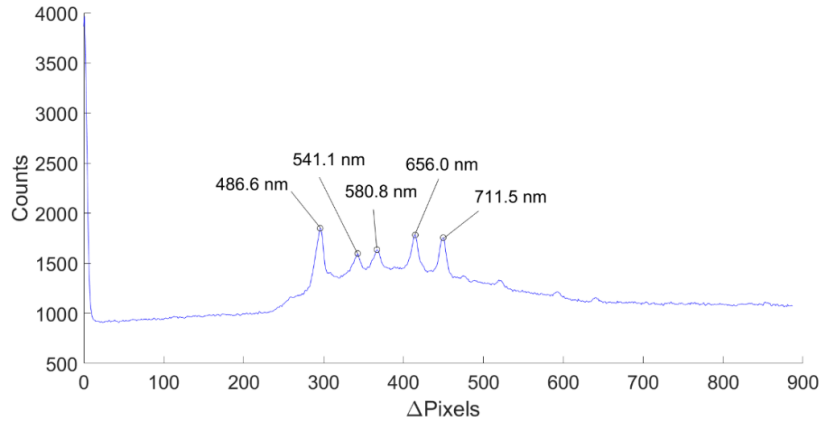


Fig. 8. Graph showing the spectrum of HD 4004 as it is recorded by the CCD array of the CMU-Falcon telescope. The known spectral features in the spectrum are used to build a relationship between Δ Pixels and wavelength. This image was taken on Jan 27th 2021.

Below in Fig. 9. is the fit generated from 16 data points for the CMU-Falcon. The measured slopes, offsets, and the 95% confidence intervals of the pixel-wavelength conversion for the diffraction gratings in the CMU-Falcon and NJC-Falcon telescopes are listed in Table 3. As expected, each telescope had extremely similar values for each star's characterization.

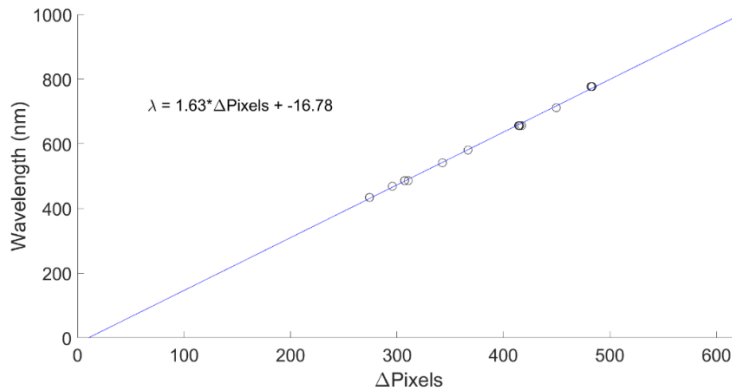


Fig. 9. Conversion fit obtained from the spectral features of multiple calibration stars for CMU-Falcon taken on Jan 27th 2021.

TABLE 3: PIXEL-WAVELENGTH CONVERSION FOR CMU-FALCON AND NJC-FALCON

	Source	Points	Slope (nm/pixels)	Offset (nm)
CMU	Alhena	4	$1.64 \pm .048$	-18 ± 6.32
	Sirius	3	$1.68 \pm .199$	-39 ± 14.13
	SAO 59570	4	$1.63 \pm .050$	-15 ± 6.71
	HD4004 (Wolf-Rayet)	5	$1.58 \pm .009$	$.8 \pm .9$
	Compiled Fit	16	$1.63 \pm .011$	-17 ± 2.38
NJC	Alhena	4	$1.64 \pm .057$	-17 ± 7.53
	Sirius	4	$1.66 \pm .052$	-26 ± 6.76
	SAO 59570	4	$1.63 \pm .069$	-14 ± 9.27
	HD4004 (Wolf-Rayet)	5	$1.60 \pm .020$	-7 ± 1.98
	Compiled Fit	17	$1.64 \pm .010$	-19 ± 2.25

By applying the conversion between pixel space and wavelength space, the spectrum from the first order interference pattern was extracted from an image. As shown below in Fig. 10 is the spectrum obtained by applying the CMU-Falcon conversion to the image of HD 4004 taken on Jan 27th 2021.

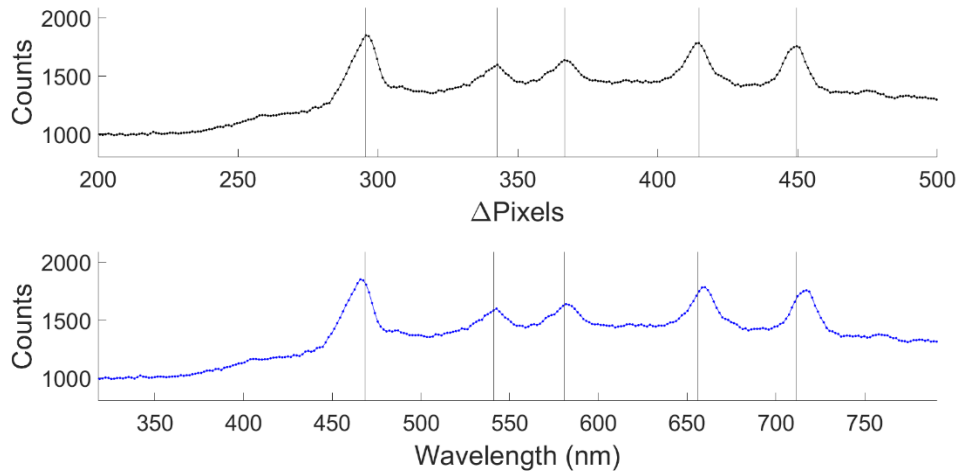


Fig. 10. Processed data for HD4004 and the spectrum obtained by applying the determined pixel-wavelength conversion for the CMU-Falcon. Note the vertical lines do not match up exactly because the conversion fit obtained from multiple stars is not the same as the conversion fit obtained from the HD 4004's data. This is annotated in Table 3.

6. CONCLUSION

The data collected across 2020-2021 and the associated photometric and spectral calibration methodology have helped to inform us of the accuracy of the FTN. Although only a subset of the data has been analyzed 20 of 63 nights. Additional statistical analysis throughout the collection period is needed to determine the accuracy of the FTN in a variety of conditions. Importantly it can be seen that there are diminishing returns in the value of collecting more calibration data beyond 6 stars. This is important as future observation plans can be adjusted accordingly as current FTN observation plans often have 50% of the telescope time devoted to collecting calibration data while the other 50% of the time is devoted to collecting target data. Reducing the number of CalStars will allow for a greater percentage of the night dedicated to observing satellites. Additional work will be done by determining the calibrated magnitudes of satellites and comparing those calibrated magnitudes from different telescope locations. Then using

the satellite observations to characterize the satellites and determine if more analysis is necessary on nightly variation in the extinction curve is warranted.

The spectral calibration slope and offsets for the CMU-Falcon and NJC-Falcon provide an accurate, but low resolution conversion from pixel space to spectral space. Additionally, the spectral calibration slopes, offsets, and confidence intervals of the CMU-Falcon and NJC-Falcon indicates that the conversion for each telescope in the FTN are extremely similar as should be expected since every Falcon telescope is identical. This means that in a large network of identical telescopes, a good conversion for all of the telescopes could be obtained by characterizing just a few of them. This process will be applied to the rest of the operational telescopes in the FTN to make them capable of spectral observations and to verify that they also have the same pixel-to-wavelength conversion equations.

7. ACKNOWLEDGEMENTS

We want to acknowledge the support of the Air Force Office of Scientific Research. Additionally, this paper is the result of multiple physics senior capstone projects and independent studies at the United States Air Force Academy since 2019. DISTRIBUTION STATEMENT A: Approved for public release: distribution unlimited. PA#: USAFA-DF-2021-237. DISCLAIMER: The views expressed in this article are those of the authors and do not necessarily reflect the official policy or position of the United States Air Force Academy, the United States Air Force, the United States Space Force, the Department of Defense, or the U.S. Government.

8. REFERENCES

- (1) *Spacepower* (Headquarters United States Space Force, 2020).
- (2) Chun, F. K. et al., “A New Global Array of Optical Telescopes: The Falcon Telescope Network,” Publications of the Astronomical Society of the Pacific, 2018.
- (3) Young, A. T., “Air Mass and Refraction: Applied Optics,” The Optical Society, 1994.
- (4) Tippetts, R. D., “Slitless spectroscopy of geosynchronous satellites,” *Optical Engineering*, 2015.